RSC Advances

ROYAL SOCIETY OF CHEMISTRY

www.rsc.org/advances

Synthesis and characterization of fluconazole-functionalized magnetic nanoparticles as a catalyst for the synthesis of 3-aryl and 3-amino-imidazo[1,2-*a*]pyridines

Mohammad Jafarzadeh,[a]* Ebrahim Soleimani,[a,b] Heshmatollah Sepahvand,[a] Rohana Adnan[c]

[a]Department of Organic Chemistry, Faculty of Chemistry, Razi University, Kermanshah 67149-67346, Iran

[b]Department of Chemistry, College of Sciences, Kermanshah Branch, Islamic Azad University, Kermanshah, Iran

[c]School of Chemical Sciences, Universiti Sains Malaysia, 11800 Minden, Penang, Malaysia

*Corresponding author (M. Jafarzadeh): Email: mjafarzadeh1027@yahoo.com

Abstract

Fluconazole was successfully immobilized on the surface of chloropropyl-modified Fe_3O_4-SiO_2 core-shell nanoparticles and was found to exhibit unique catalytic activity for the synthesis of 3-aryl-imidazo[1,2-*a*]pyridines in water. This catalyst also showed great activity in a multi-component reaction for the synthesis of 3-amino-imidazo[1,2-*a*]pyridines under solvent-free conditions. The magnetically-recoverable catalyst was found to be capable of repeated reuse without significant loss of activity.

Keywords: Fluconazole, Magnetic silica nanoparticles, Triazole, Imidazo[1,2-*a*]pyridine

1. Introduction

Magnetic silica nanoparticles have recently received significant attention due to their chemical inertness, magnetic properties, nontoxicity, and excellent thermal stability.[1] These favorable properties allow nanoparticles (NPs) to be widely used as a catalyst or catalyst support for organic syntheses.[2] However, a major drawback in using homogeneous catalysts is the difficulty of catalyst isolation from the reaction media and their reusability. Heterogenation of organic catalysts through immobilization on the surface of inert materials is a common way to overcome these problems. Organo-functionalization of silica allows researchers to customize the surface with a wide variety of active organic compounds and organic catalysts. For catalytic applications, the reaction of silica-based materials with organohalotrialkoxysilane is a common method for the initial functionalization of the support by a post-modification process.[3] The covalent linkage of the organic groups to the silica surface by reaction with organohalotrialkoxysilane has been widely reported in the literature.[4]

Fluconazole (FLU) or 2-(2,4-difluoro-phenyl)-1,3-bis-[1,2,4]triazol-1-yl-propan-2-ol, is a bis-triazole antifungal commonly utilized to treat invasive infections.[5] The structure of FLU consists of two triazole rings, with the nitrogen atoms of the triazoles demonstrating nucleophilic behavior through their lone pair electrons. It is expected that the reaction between the nitrogen of the triazole ring and the halogen functional group of the organosilane can be carried out via a nucleophilic substitution reaction, and that the functionalized silica materials can be employed as a catalyst in organic synthesis.

A variety of materials such as organic amines, inorganic bases, and ionic liquids have been used as catalysts for the synthesis of imidazo[1,2-*a*]pyridines, respectively.[6] Bangade et al. reported synthesis of 3-aryl-imidazo[1,2-*a*]pyridines in the presence of 1,4-diazabicyclo[2.2.2]octane (DABCO) under an aqueous medium.[6b] Shaabani et al. prepared 3-amino-imidazo[1,2-*a*]pyridines in an ionic liquid medium[6c] and Daemi et al. applied the cationic polyurethane dispersion in this reaction.[6f] In our work, the grafting of FLU onto the surface of magnetic silica core-shell nanostructures is carried out. The catalytic activity of these nanostructures is examined for the synthesis of 3-aryl and 3-amino-imidazo[1,2-*a*]pyridines and the catalyst is separated from the reaction mixture using a magnet and reused for several cycles. The use of FLU as a homogeneous or heterogeneous catalyst has not been previously reported.

2. Experimental

Tetraethoxysilane (TEOS, 99%), chloropropyltriethoxysilane (CPTES, 99%) and absolute ethanol (EtOH, 99%) were purchased from Merck and used without further purification. Fluconazole was purchased from Pars Daru Company.

2.1. Preparation of modified silica coated magnetite NPs (Fe_3O_4@SiO_2~Cl)

Magnetite (Fe_3O_4) nanoparticles (NPs) were prepared according to the reported method (co-precipitation)[7] and coated with silica in the presence of 2-propanol (sol-gel method[8]). In brief, 0.036 mol of $FeCl_3.6H_2O$ and 0.018 mol of $FeCl_2.4H_2O$ were dissolved in 20 mL deionized water under nitrogen gas with vigorous stirring. Then, NH_3 (25%) was added into the solution until the pH of the solution reached 11. Stirring was continued for 1 h at 60 ºC. The color of the bulk solution turned from orange to black immediately. The magnetite precipitate was separated from the solution using a magnet, washed several times with deionized water and ethanol, and left to dry in air. Then, 30 mg as-synthesized Fe_3O_4 NPs were mixed with 50 mL isopropyl alcohol in a sealed three-neck flask by ultrasonic treatment for 30 min. 10 mL deionized water, 0.3 mL TEOS (silica precursor), and 1.70 mL ammonia (25 wt%) were added into the mixture of Fe_3O_4 and isopropyl alcohol at 30 °C under mechanical agitation. After 12 h, the final product (Fe_3O_4@SiO_2) was collected, washed with ethanol and deionized water and dried at 50 ºC. The silica coated Fe_3O_4 (Fe_3O_4@SiO_2) NPs were then functionalized using a post-modification method with 3-

chloropropyltriethoxysilane (CPTES)[9] by refluxing in anhydrous toluene at 110 °C for 24 h (Fe_3O_4@SiO_2~Cl).

2.2. Immobilization of fluconazole on the surface of modified silica-coated magnetite NPs (Fe_3O_4@SiO_2~Flu)

The fluconazole (3 g, 10.79 mmol) was added into a suspension of Fe_3O_4@SiO_2~Cl powder (1.0 g) in dry DMF (30 mL). The reaction mixture was refluxed at 140 °C in an oil bath for 24 h. The solid phase was filtered and washed with DMF, followed by distilled water. Finally, the solid sample was dried at 100 °C for 24 h.

2.3. Characterization techniques

Infrared spectra were recorded using a Ray Leigh Wqf-510 Fourier Transform Infrared (FTIR) spectrophotometer. Morphological studies measurements were performed using a Transition Electron Microscopy (TEM, Philips CM10) operated at an 80 kV electron beam accelerating voltage. Scanning electron microscopy (SEM) and EDX were performed on a Philips XL-300 instrument. The sample was sputtered by gold to avoid undesirable electron charging. X-ray diffraction was conducted using a Philips X'pert Pro (PW 3040) X-ray diffractometer with monochromatic Cu-Kα radiation (k = 1.54056 Å, 40 kV, 30 mA). Particle size distribution and zeta potential were obtained using a Malvern Zetasizer (Nano ZS series - Model: ZEN3600). Ultraviolet-visible (UV-Vis) absorption spectra were recorded on a Perkin-Elmer Lambda 25. Thermogravimetric analyses were investigated using a TG/DTA6300 instrument, at a heating rate of 20 °C min^{-1} under nitrogen flow. Elemental analysis was performed with a CHN machine (Perkin Elmer Series II, 2400). ^1H and ^{13}C NMR spectra were recorded on a Bruker DRX-400 spectrometer at 400 and 100 MHz, respectively.

2.4. General procedure for the synthesis of 3-aryl-imidazo[1,2-*a*]pyridines

A mixture of phenacyl bromide (1 mmol), 2-aminopyridine (1 mmol), and an appropriate amount of Fe_3O_4@SiO_2~FLU was stirred in water (5 mL) at 60–70 °C for 1 h. The reaction progress was monitored by TLC (Thin Layer Chromatography) using silica gel polygram SIL G/UV 245 plates. After the completion of the reaction, the catalyst was separated by applying an external magnet and extracted with ethyl acetate (3×5 mL). The combined organic layer was washed with brine solution, dried over anhydrous Na_2SO_4 and concentrated under reduced pressure. All known products were characterized by comparison of their spectral data and physical properties (including the melting point) with those reported in the literature. The new derivative compounds were characterized by ^1H and ^{13}C NMR. The following is the spectral data of 3-phenyl-7-methyl-imidazo[1,2-a]pyridine **(3b)** and 3-(4-bromo phenyl)-7-methyl-imidazo[1,2-a]pyridine **(3f)**, which were prepared via reaction of 2-amino-3-methylpyridine with phenacyl bromide and 4-bromophenacyl bromide, respectively (refer to Table 2 in Part 3.2).

8-Methyl-3-phenylH-imidazo[1,2-a]pyridine (3b): Yellow solid. mp 144-146 ^{o}C; ^{1}H NMR (400 MHz, DMSO-d_6): δ_H (ppm) 2.66 (3H, s, CH_3), 7.4 (1H, s, CH of imidazole ring), 7.73–7.56 (4H, m, H-Ar), 7.99 (2H, m, H-Ar), 8.75 (2H, m, H-Ar). ^{13}C NMR (100 MHz, DMSO-d_6): δ_C (ppm) 16.3 (CH_3), 111.6, 116.9, 126.4, 126.7, 127.5, 128.6, 129.3, 130.1, 131.9, 133.9, 141.6.

6-Bromo-8-methyl-3-phenylH-imidazo[1,2-a]pyridine (3f): Yellow solid. mp 152–154^{o}C; ^{1}H NMR (400 MHz, DMSO-d_6): δ_H (ppm) 2.66 (3H, s, CH_3), 7.4 (1H, s, CH of imidazole ring), 7.82–7.97 (4H, m, H-Ar), 8.71 (2H, m, H-Ar). ^{13}C NMR (100 MHz, DMSO-d_6): δ= 16.3 (CH_3), 111.8, 116.3, 126.2, 126.6, 128.3, 129.4, 130.7, 132.1, 136.3, 151.6, 156.0.

2.5. General procedure for the synthesis 3-amino-imidazo[1,2-*a*]pyridines.

To the mixture of aldehyde (1.0 mmol), 2-aminopyridine (1.0 mmol), and isocyanide (1.2 mmol), 0.1 g of Fe_3O_4@SiO_2~FLU NPs was added. The resulting mixture was stirred at 60 ˚C under solvent-free conditions. After completion of the reaction, as indicated by TLC (ethyl acetate/n-hexane, 2:1), ethanol was added to the reaction mixture, and an external magnet was applied to separate the catalyst. The solvent was removed under vacuum and the residue was crystallized from ethyl acetate to obtain the product.

All known products were characterized by comparison of their spectral data and physical properties with those reported in the literature.

2.6. Recovery of the catalyst

After the catalyst was separated from the reaction medium by applying an external magnetic field, it was thoroughly washed with ethanol and activated by heating at 100 °C for 1 h in an oven. The catalyst was found to retain most of its catalytic activity after recycling and recovering. The supported organocatalyst stability and catalyst regeneration were determined by FTIR.

3. Results and discussion

3.1. Preparation and characterization of the catalyst

The Fe_3O_4@SiO_2~FLU nanocatalyst was prepared with a multi-step reaction - initially by preparing iron oxide as a magnetic core for coating by a silica layer through sol-gel process. For immobilization of the organic catalyst on the surface of inorganic support, the surface was first modified using an appropriate coupling agent to make covalent bonds with the catalyst. It is known that organosilanes can act as a linker between the organic catalyst and the support. In this work, chloropropyltriethoxysilane was used. Scheme 1 illustrates the process of catalyst preparation. A part of the linker's chloride was replaced by nitrogen of the

triazole via an S_N2 nucleophilic substitution reaction. This is because the chloropropyl group provides type 1 alkyl halide, allowing the nucleophile (triazole) to attack the carbon containing Cl, and to release the chloride as a leaving group. Each step of the catalyst preparation procedure was monitored using techniques such as FTIR to ensure the presence of new functional groups.

There is also the potential for both triazole rings to attach to the surface. The chloride ions resulting from the nucleophilic substitution by nitrogen of triazole are formed from ammonium/chloride ion pairs. The quaternary ammonium, with its corresponding counter ion, can form ionic liquid (IL) on the surface. This type of solid supported ionic liquid (i.e. Supported Ionic Liquid Phase (SILP) catalysts[10,11]) is expected to show specific task, as a catalyst/medium, in organic synthesis. The central carbon of FLU is prochiral, which can be converted to chiral centers upon the immobilization of FLU on the surface of the support. The formation of stereoisomeric carbon in the center of the FLU structure also has potential applications in asymmetric syntheses.[12,13] Work is currently underway in our lab to develop this catalyst in asymmetric synthesis and other synthetic methodologies.

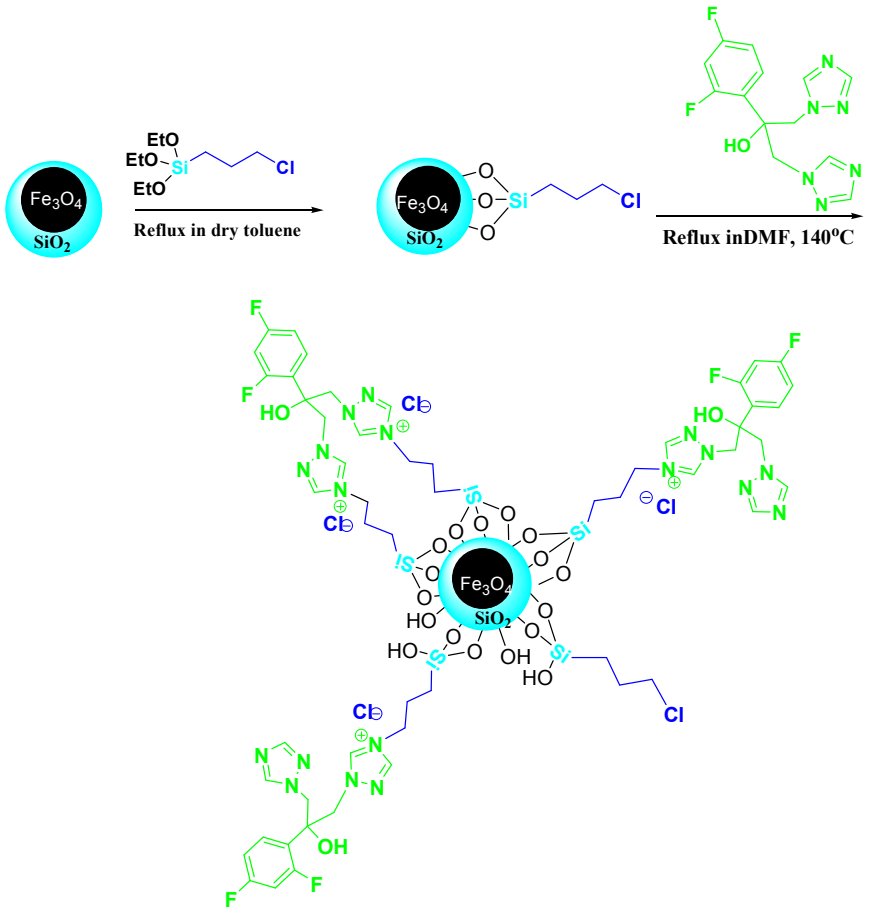

Scheme 1. The schematic pathway for immobilization of fluconazole on the surface of Fe_3O_4@SiO_2~Cl core-shell nanoparticles.

The crystalline structure of magnetite nanoparticles (before and after silica coating) was identified with the XRD technique. Figure 1 shows the XRD patterns of Fe_3O_4, Fe_3O_4@SiO_2, Fe_3O_4@SiO_2~Cl, and Fe_3O_4@SiO_2~FLU. For Fe_3O_4 diffraction peaks at different angles (2θ) were attributed to the corresponding planes of cubic spinel Fe_3O_4, and are in good agreement with the reported XRD patterns of Fe_3O_4 NPs.[14] The silica–coating process and further functionalization with CPTES and FLU did not influence the crystalline structure of the Fe_3O_4 core. Therefore, similar XRD pattern to that of Fe_3O_4 were also observed for Fe_3O_4@SiO_2, Fe_3O_4@SiO_2~Cl and Fe_3O_4@SiO_2~FLU. The (311) XRD peak was used to determine the mean nanoparticle diameter by Scherrer's equation $D = 0.9\ \lambda/(\beta \cos\theta)$, where D is the average crystalline size, λ is the wavelength (Cu Kα, 1.54 Aº), β is the angular line width of half-maximum intensity (full width at the half-maximum FWHM), and θ is the Bragg's diffraction angle in degrees.[15] The mean crystallite size calculated was 27 nm.

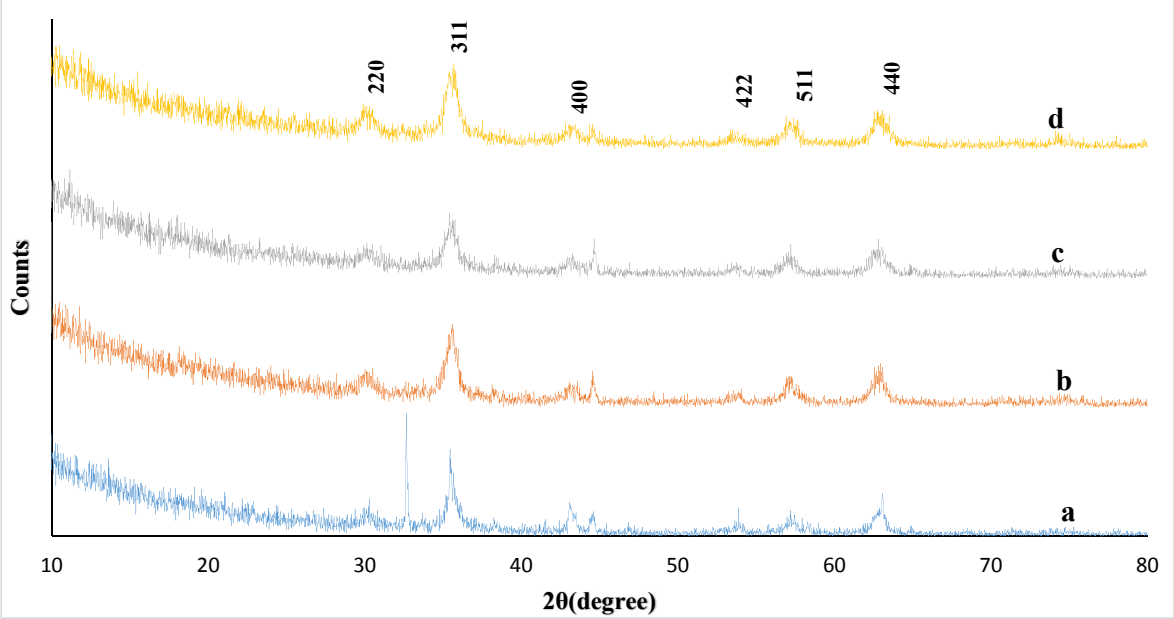

Figure 1. XRD patterns of (a) Fe_3O_4, (b) Fe_3O_4@SiO_2, (c) Fe_3O_4@SiO_2~Cl and (d) Fe_3O_4@SiO_2~FLU NPs.

Figure 2 shows the particle size distribution obtained using Dynamic Light Scattering (DLS). The z-average hydrodynamic diameter of Fe_3O_4, Fe_3O_4@SiO_2~Cl, and Fe_3O_4@SiO_2~FLU NPs dispersed in ethanol were about 174 nm (87 r.nm; radius nanometer, PdI=1.00), 438.6 nm (219.3 r.nm, PdI=0.405), and 470.0 nm (235.0 r.nm, PdI=0.331), respectively. These results indicated that there is aggregation among NPs in colloidal form. The diameters measured by DLS for modified magnetite NPs were larger than the initial magnetic NPs due to differences in their dispersion properties in ethanol. After organo-functionalization, the nature of the surface varied from hydrophilic to hydrophobic and thus the type of interaction between the catalyst surface and the solvent (ethanol) changed upon modification. The difference between the DLS and XRD diameters were due to differences in size measurement techniques and sample preparations; the size

calculated by XRD was related to the size of crystallites, whereas DLS gave the dynamic size of aggregated and agglomerated particles. The DLS generally shows larger particle size than that in TEM and it was inferred that this was a result of the surface charge of the nanoparticles affecting the hydrodynamic size measurement of the sample in colloidal form. In contrast, dried samples are generally used for TEM analysis.[16] By increasing the number of hydrophilic groups on the surface, the probability of undesirable agglomeration among nanoparticles increases. In addition, the existence of ionic bonds between quaternary ammonium of triazole rings and chloride groups (ionic liquid form) in Fe_3O_4@SiO_2~FLU NPs further enhance the polarity of the shell.

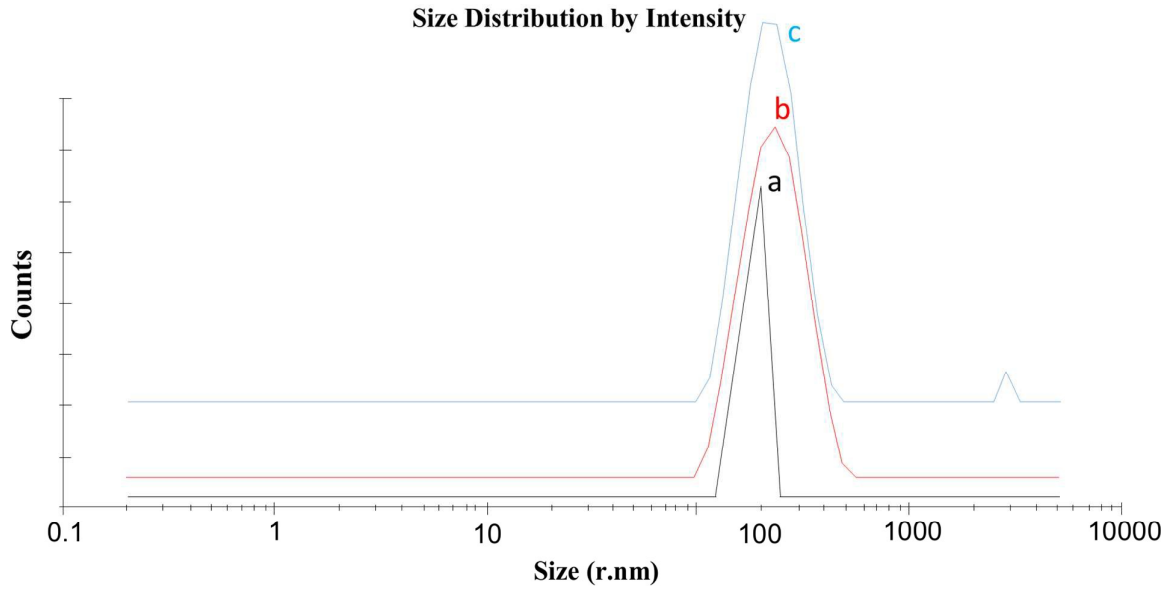

Figure 2. Particle size distribution of (a) Fe_3O_4, (b) Fe_3O_4@SiO_2~Cl and (c) Fe_3O_4@SiO_2~FLU NPs.

Transmission electron microscopy (TEM) was used to observe the morphology of the three-stage synthesis of the catalyst. Figure 3(a) shows that the NPs have a core-shell structure with a distinct contrast between silica shells and Fe_3O_4 cores, implying that silica shells (Fe_3O_4@SiO_2) successfully coated the hydrophilic Fe_3O_4 NPs. The average size of the cores was found to be ~25-30 nm – a result consistent with the crystallite size of 25 nm for Fe_3O_4 NPs obtained from XRD. The thickness of the silica shell was estimated to be around 10-15 nm. Therefore, the average size of magnetite-silica core-shell nanoparticles was determined to be around ~35-45 nm Similarly, the TEM images of Fe_3O_4@SiO_2~Cl, and Fe_3O_4@SiO_2~FLU are shown in Figures 3(b) and 3(c), respectively. These images reveal that the modified magnetic silica nanoparticles and Fe_3O_4@SiO_2~FLU are similar in size (~40-45 nm) and are spherical in shape. The Scanning Electron Microscopy (SEM) image of Fe_3O_4@SiO_2~FLU in Figure 3(d) show the granular and spherical morphology for these nanoparticles. The average size of 44±9.3 nm obtained by SEM analysis is consistent with the TEM results. The slight size differences between TEM and SEM results could be related to the different

sample preparations techniques, which applied to TEM (colloidal form of dried sample) and SEM (powder form with Gold thin layer sputtering).

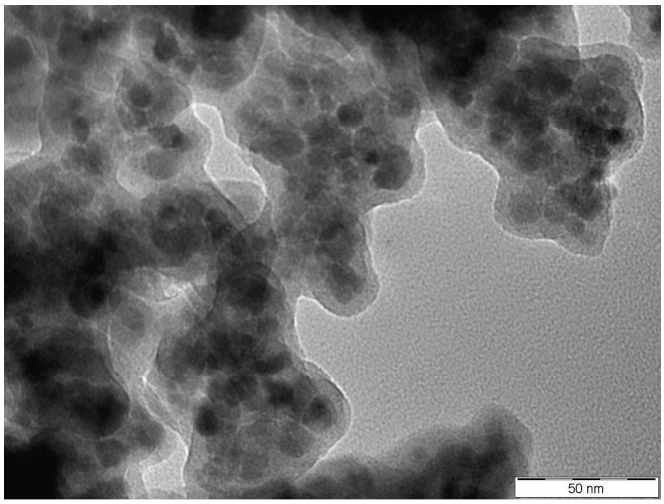

(a)

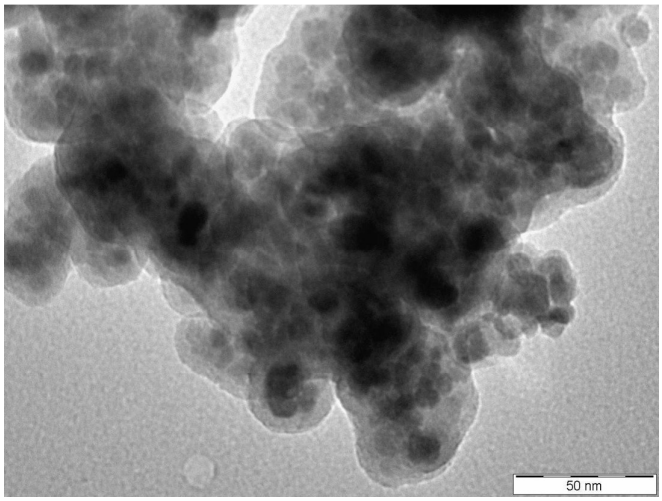

(b)

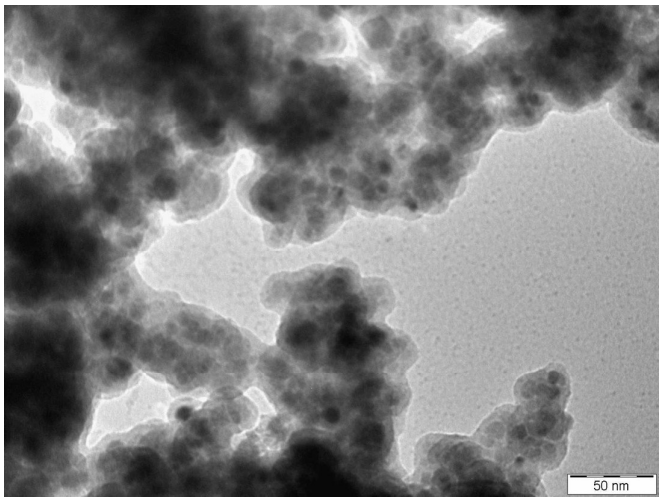

(c)

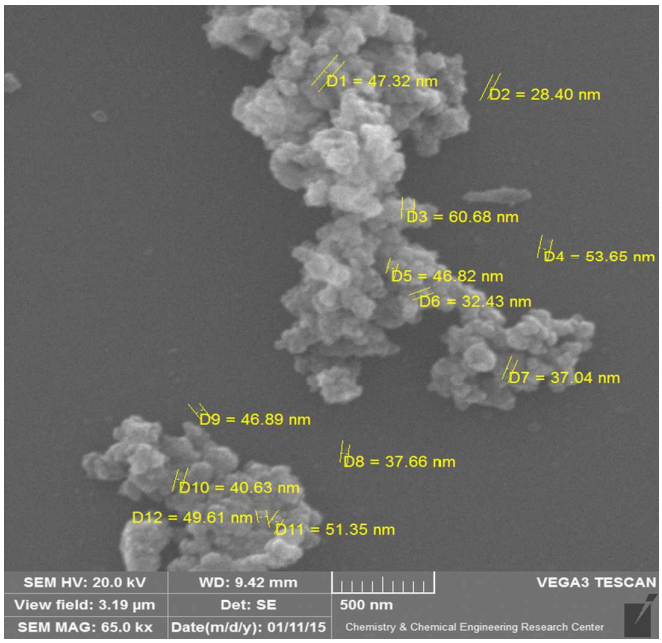

(d)

Figure 3. TEM images of (a) Fe_3O_4@SiO_2, (b) Fe_3O_4@SiO_2~Cl and (c) Fe_3O_4@SiO_2~FLU and (d) SEM image of Fe_3O_4@SiO_2~FLU.

In addition, the stages of the catalyst formation were tracked by FTIR spectroscopy. Figure 4(a) shows the FTIR spectra of the Fe_3O_4, the silica-coated Fe_3O_4, and the Fe_3O_4@SiO_2~Cl NPs. The peaks appearing at 645 cm^{-1}, 591 cm^{-1} and 445 cm^{-1} are ascribed to the stretching vibrations of Fe–O bonds, while the absorption peak at 3253 cm^{-1} is the OH stretching vibration characteristic peak, indicating the presence of some amount of ferric hydroxide in Fe_3O_4.[17] At room temperature, Fe^{2+} and Fe^{3+} are converted into hydroxide compounds with a pH above 10 (required pH for magnetite preparation is 11), while at elevated temperature (e.g. 60 ºC within magnetite preparation) they are crystallized to Fe_3O_4 slowly.[18] Silica-coated

Fe_3O_4 is expected to produce a corresponding peak of Fe–O–Si bonds at 584 cm^{-1} resulting from the adsorption of silica on the magnetite surface, while this band was overlapped with the Fe–O vibration. In other words, the formation of Fe-O-Si bonds upon silica coating affected the position of Fe-O bands, and a peak shift occurred.[19] The Si–O–Si stretching and bending vibrations appeared at 1088 cm^{-1} and 463 cm^{-1}, respectively. The absorption bands at 3460 cm^{-1}, 1100 cm^{-1} and 960 cm^{-1} are attributed to the stretching, asymmetric stretching, and bending of silanol groups (Si–OH) on the silica surface, respectively.[20] Vibrations at 3500–3400 cm^{-1}, 1637 cm^{-1} and 800 cm^{-1} correspond to the adsorbed water (H–OH, stretching vibration), residual intermolecular water (H–OH, bending), and moisture (H–OH, bending) in the samples.[3a] The spectrum of the Fe_3O_4@SiO_2~Cl shows peaks at 2847 cm^{-1} and 2926 cm^{-1} due to C–H bonds of CPTES stretching vibrations, while peaks at 638 cm^{-1} and 689 cm^{-1} indicate the presence of C–Cl bonds in CPTES.

The FTIR spectra of fluconazole and Fe_3O_4@SiO_2~FLU are shown in Figure 4(b). The spectrum of the commercially-available sample of the fluconazole showed some broad and sharp bands due to O-H stretching vibration at 3434 cm^{-1}, aromatic C=N stretching vibration at 1620 cm^{-1}, aromatic C=C stretching vibration at 1516 cm^{-1}, and C-F stretching vibration at 1273 cm^{-1}.[5] Furthermore, the absorbance of C-N and aromatic C-F were apparent at 1040 cm^{-1} and 1236 cm^{-1}, respectively. For Fe_3O_4@SiO_2~FLU, the major peaks of FLU overlapped with broad and strong bands of Si-O-Si, intermolecular water and moisture (H–OH, bending) in the samples. Therefore, CHN, EDX and TGA analyses were required to confirm the functionalization processes and the presence of FLU on the surface.

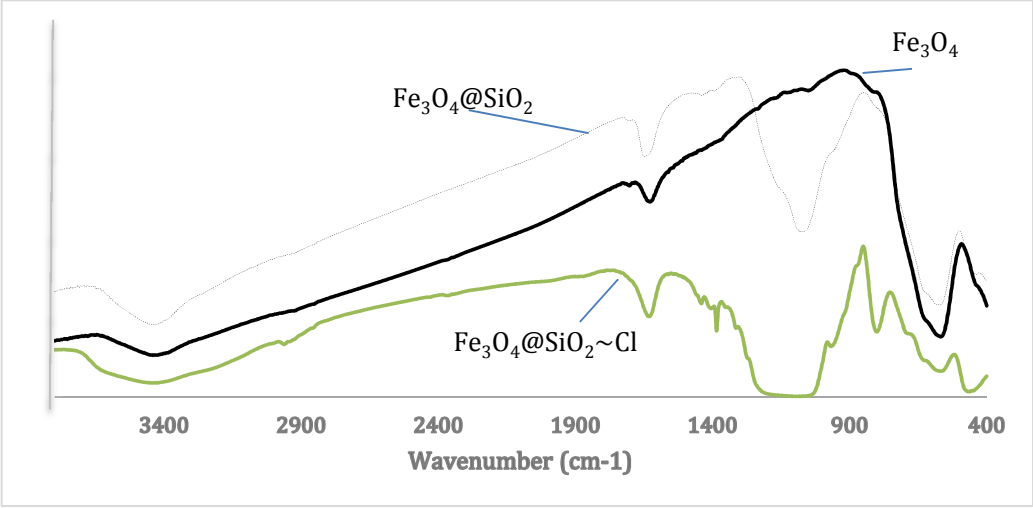

(a)

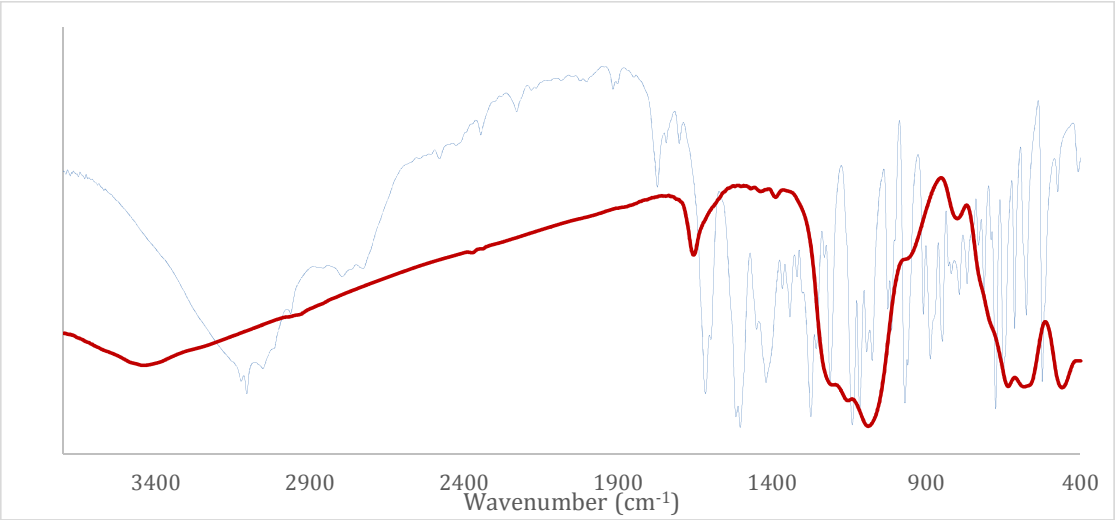

(b)

Figure 4. FTIR spectra of (a) Fe_3O_4, Fe_3O_4@SiO_2, Fe_3O_4@SiO_2~Cl, and (b) Fe_3O_4@SiO_2~FLU (red line) and fluconazole.

From the elemental analysis (CHN) in Table 1, it is observed that there is an increase in carbon content and also in hydrogen and nitrogen content after functionalization of the Fe_3O_4@SiO_2~Cl with fluconazole. This indicates the successful attachment of organic fragments (FLU) onto the surface of the modified nanoparticles. Furthermore, the Energy dispersive X-ray spectroscopy (EDX) in Figure 5 confirmed the presence of FLU with elemental analysis of Fe (74.41%), Si (3.13%), O (17.86%), C (2.76%), N (0.91%), F (0.30%), and Cl (0.63%).

Table 1. The CHN results for Fe_3O_4@SiO_2~Cl and Fe_3O_4@SiO_2~FLU.

Elements (mg/g)	Fe_3O_4@SiO_2~Cl	Fe_3O_4@SiO_2~FLU
N	0	5.712
C	30.232	43.912
H	2.071	6.426

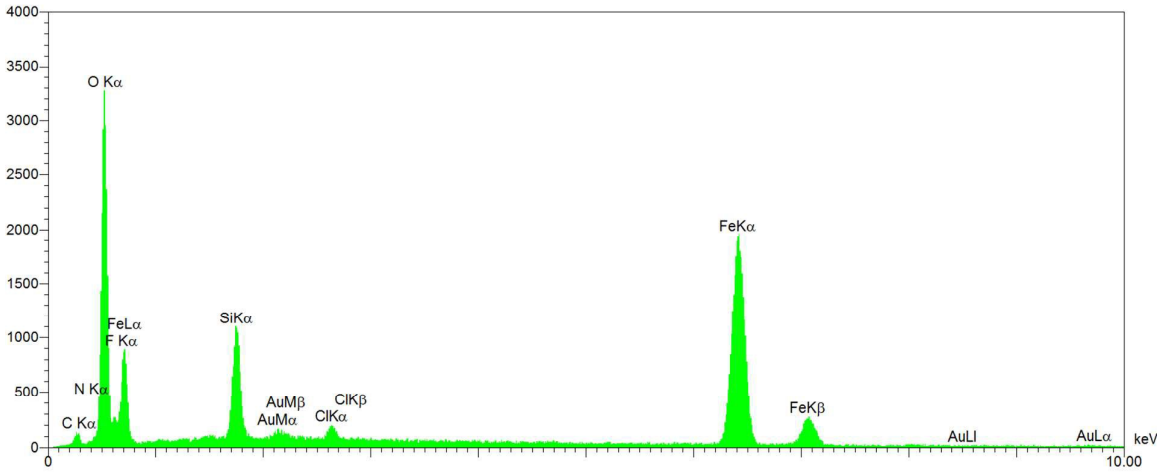

Figure 5. EDX spectrum of Fe_3O_4@SiO_2~FLU.

Thermogravimetric analysis and derivative curves (TGA/DTG) of Fe_3O_4@SiO_2~Cl and Fe_3O_4@SiO_2~FLU nanoparticles are presented in Figure 6. The initial % wt losses below 150 ^oC are related to the adsorbed moisture in the samples. The decomposition temperature, which started at ~415 ^oC, and continued until ~540 ^oC, is associated with the decomposition of the organic chains. The organic species decomposed completely at temperatures higher than 600 ^oC and the residual weights of Fe_3O_4@SiO_2~Cl and Fe_3O_4@SiO_2~FLU were ~90% and ~86%, respectively, at 700 ^oC. In other words, the results demonstrate percentages of ~4% and ~9% for organic groups on the surface of Fe_3O_4@SiO_2~Cl and Fe_3O_4@SiO_2~FLU, respectively. The differences between these two values confirm the successful immobilization of FLU on the surface of chloropropyl-modified silica coated magnetite nanoparticles. Fe_3O_4@SiO_2~FLU also exhibited a slight weight loss in the temperature range of ~200-300 ^oC that can be related to the partial degradation of FLU. This phenomenon was not observed for Fe_3O_4@SiO_2~Cl.

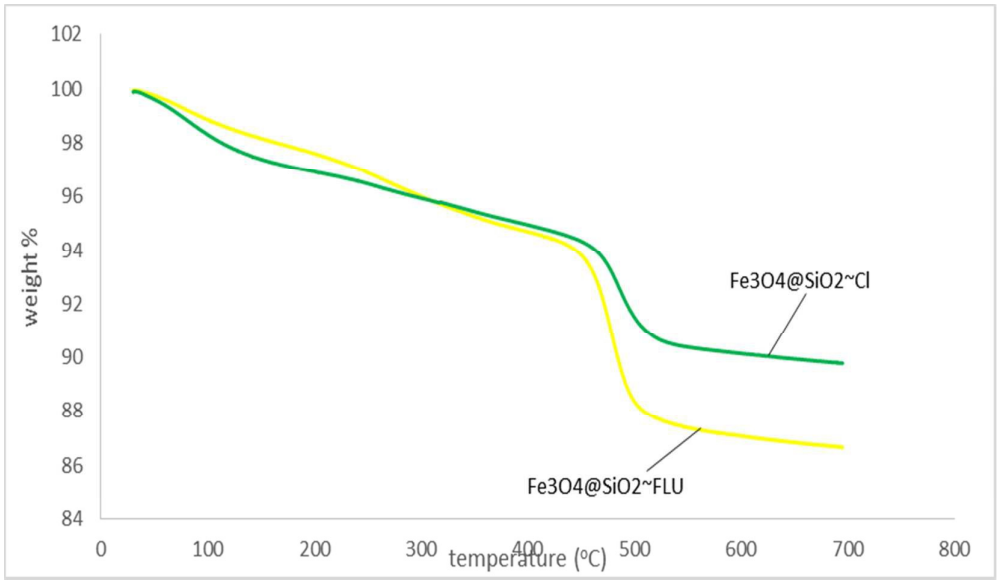

(a)

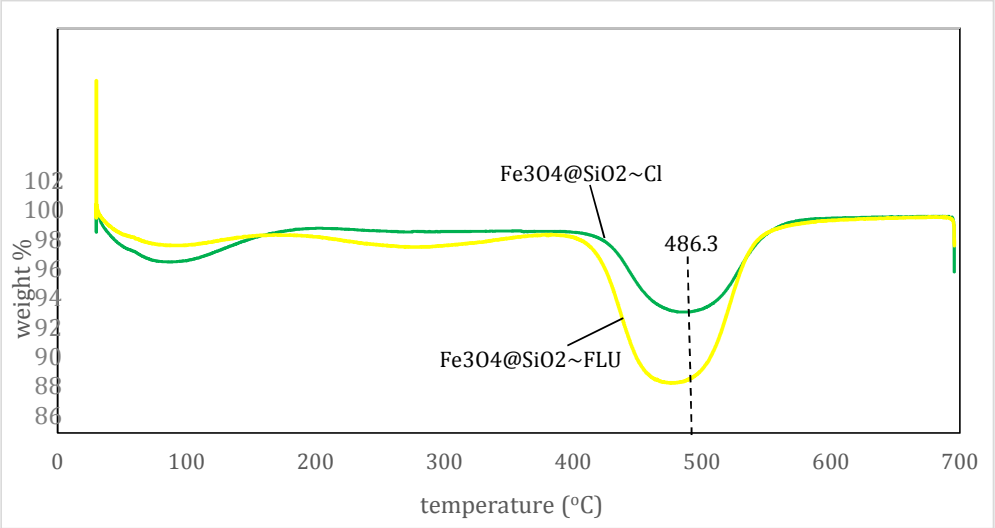

(b)

Figure 6. (a) TGA and (b) DTG curves of Fe_3O_4@SiO_2~Cl before and after FLU functionalization.

The measurement of zeta (ζ) potential was performed in order to study the variation of surface charge after the modification of silica with chloropropyltriethoxysilane and immobilization of FLU. The zeta potential is the electric potential in the interfacial double layer between the dispersion medium and the stationary layer of fluid besides the dispersed particles.[21] The surface charge of silica in Fe_3O_4@SiO_2 was negative, arising from $Si–O^-$ groups, and the zeta potential was -2.26. These values reduced to -1.96 and -1.72 upon functionalization of the silica surface with CPTES and FLU groups, respectively. This further confirms the introduction of organic groups onto the silica surface, and that the nature of the surface changed from hydrophilic to hydrophobic depending on the quantity of surface modification. The observed negative charge after modification might be due to the existence of un-modified silanol (Si–OH) groups, the effect of steric hindrance of organic chain to avoid further surface modification, and also on the existence of ionic liquid nature on the surface upon FLU immobilization. Due to the large structures in FLU and the existence of three rings that cause hindrance and steric repulsion between the FLU molecules, the replacement of all chlorides is impossible. In other words, after attachment of FLU to the CPTES, the proximity of further FLU to the surface is constrained. Therefore, limited immobilization of FLU on the surface leads to a slight reduction in surface charge. In contrast, the formation of ionic pairs between the triazole ring of FLU and the chloride released upon immobilization enhances the surface charge.

3.2. Catalytic activity of Fe_3O_4@SiO_2~FLU in organic synthesis

The fluconazole-immobilized magnetic nanocatalyst was employed for the synthesis of 3-aryl-imidazo[1,2-*a*]pyridines. Scheme 2 demonstrates the reaction between phenacyl bromides and 2-aminopyridine in the presence of the catalyst at 60 °C in water. To find the optimum conditions, different amounts of the catalyst

(0.03-0.1 g) were used for the model synthesis (entry 1-4, Table 2). The highest yield (92%) was obtained within 1 h using 0.07 g of the catalyst. Although 0.07 g of the catalyst produced the highest yield, poor reusability and lower yield in subsequent runs were observed with this amount, due to higher agglomeration and aggregation of the catalyst during isolation. Instead, the amount of 0.05 g, producing a reasonable yield (90%), was finally selected for further studies. Different derivatives of the starting materials were employed to generalize this synthetic protocol. Phenacyl bromides with electron-withdrawing groups showed higher yield than the compound with electron-donating groups. Furthermore, the steric effect arising from the presence of methyl groups in R2 of aminopyridine lowered the reactivity of the amine group in the reaction. The catalyst was successfully recycled and reused several times without significant loss of its activity, as demonstrated in Figure 7.

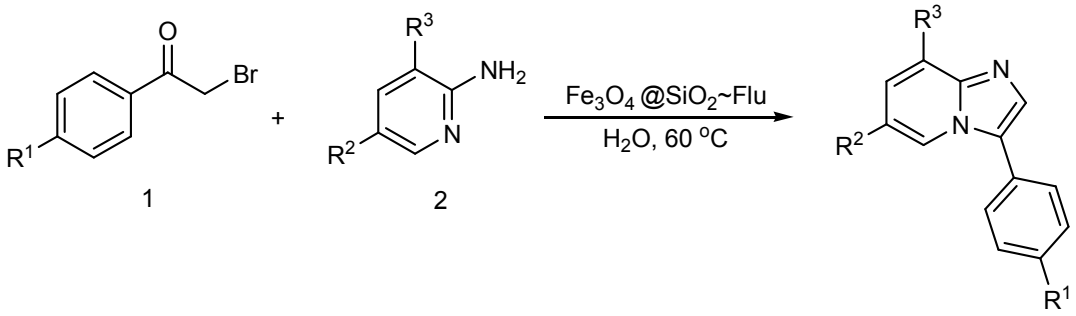

Scheme 2. Synthesis of 3-aryl-imidazo[1,2-*a*]pyridines.

Table 2. Optimization of the reaction condition for the synthesis of 3-aryl-imidazo[1,2-*a*]pyridines.[a]

Entry	R^1	R^2	R^3	Catalyst (g)	Product	Time (h)	Yield (%)[b]
1	H	H	H	0.03	**3a**	1	70
2	H	H	H	0.05		1	90
3	H	H	H	0.07		1	92
4	H	H	H	0.10		1	92
5	H	H	Me	0.05	**3b**	2	94
6	MeO	H	H	0.05	**3c**	1.5	82
7	MeO	Me	H	0.05	**3d**	1.5	85
8	Br	H	H	0.05	**3e**	1	94
9	Br	H	Me	0.05	**3f**	2	96
10	NO_2	H	H	0.05	**3g**	1	96
11	NO_2	Me	H	0.05	**3h**	1	91

[a]Reaction condition: phenacylbromide (1 mmol), 2-aminopyridine (1.2 mmol) and the catalyst in H_2O (5 mL) at 60 °C. [b]Isolated yields

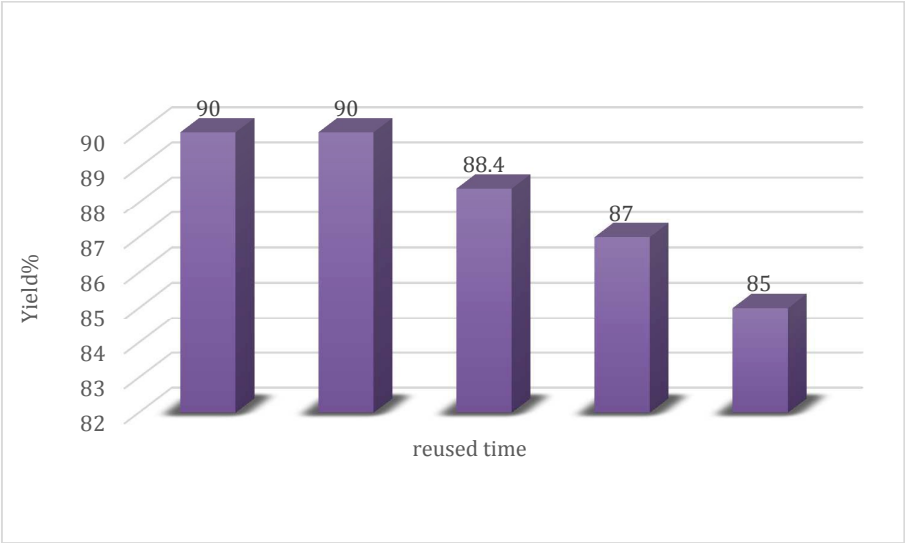

Figure 7. Reusability of the catalyst for synthesis of 3-phenyl-imidazo[1,2-*a*]pyridine (model reaction: entry 3, Table 2).

The FLU-immobilized magnetite-modified silica core-shell nanocatalyst was also utilized for the synthesis of 3-amino-imidazo[1,2-*a*]pyridines. A multi-component reaction involving condensation of benzaldehydes, 2-aminopyridines, and isocyanide was carried out for this synthesis. To determine the optimum reaction parameters, benzaldehydes, 5-methyl-2-aminopyridines, and cyclohexyl-isocyanide were chosen as a model reaction in the presence of different amounts of the catalyst (0.03-0.15 g) at 60 ˚C in solvent-free conditions (Scheme 3). The results show a 98% yield by using only 0.1 g of the catalyst (Fe_3O_4@SiO_2~FLU) after 1 h of reaction time (entry 3, Table 3). A variety of different benzaldehydes, with electron-withdrawing and electron-donating groups, exhibited good yields (94-99%). *Tert*-butyl isocyanides required longer reaction times to afford a yield above 90%. The supported catalyst was easily recovered by applying an external magnetic field, and successfully reused several time without significant loss of reactivity (Figure 8).

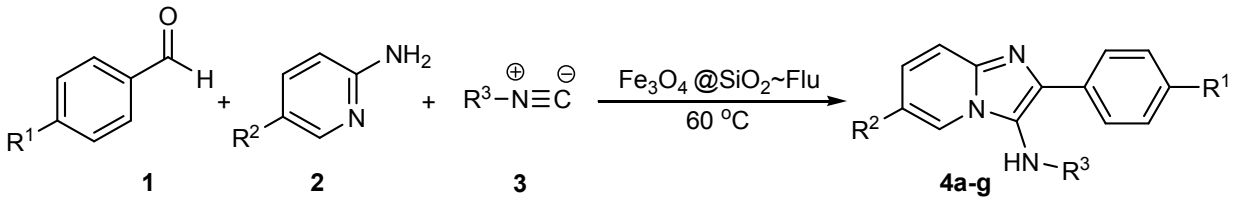

Scheme 3. Synthesis of 3-amino-imidazo[1,2-*a*]pyridines.

Table 3. Optimization of the reaction condition for the synthesis of 3-amino-imidazo[1,2-*a*]pyridine.[a]

Entry	R^1	R^2	R^3	Catalyst (g)	Product	Time (h)	Yield (%)[b]

1	H	Me	Cyclohexyl	0.03	**4a**	1	60
2	H	Me	Cyclohexyl	0.05		1	75
3	H	Me	Cyclohexyl	0.10		1	98
4	H	Me	Cyclohexyl	0.15		1	90
5	Me	Me	Cyclohexyl	0.10	**4b**	1	99
6	Cl	Me	Cyclohexyl	0.10	**4c**	1	94
7	NO_2	Me	Cyclohexyl	0.10	**4d**	1	97
8	H	Br	Cyclohexyl	0.10	**4e**	1	98
9	H	Me	*tert*-Butyl	0.10	**4f**	1.5	93
10	Me	Me	*tert*-Butyl	0.10	**4g**	1.5	90

[a]Reaction condition: benzaldehyde (1 mmol), aminopyridine (1 mmol), isocyanide (1 mmol) and Fe_3O_4@SiO_2~FLU at 60°C in solvent-free condition. [b]Isolated yields

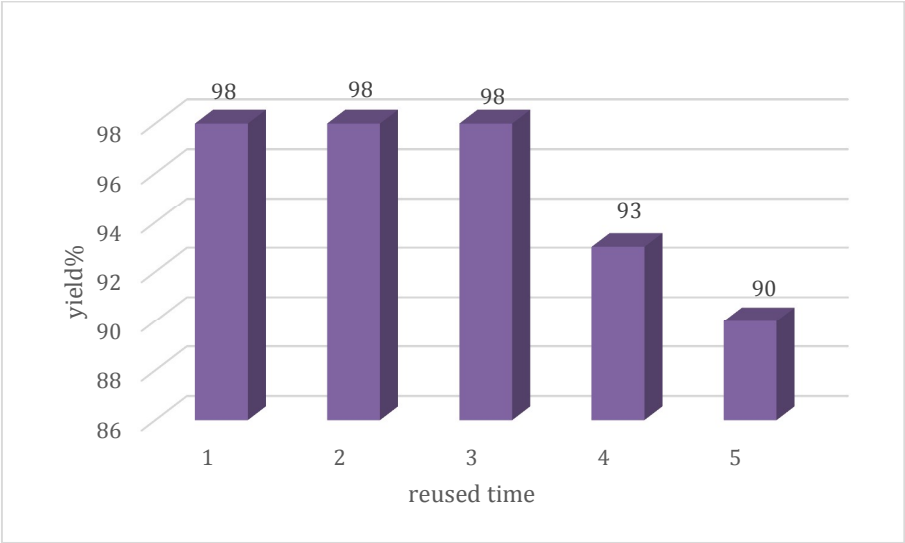

Figure 8. Reusability of the catalyst for synthesis of 3-amino-imidazo[1,2-*a*]pyridine (model reaction: entry 3, Table 3).

Catalyst stability

Comparison between the FTIR spectra of the as-prepared (fresh) catalyst and the reused catalyst in Figure 9 demonstrated great stability of the catalyst in both of the preceding syntheses, without change in surface functionality.

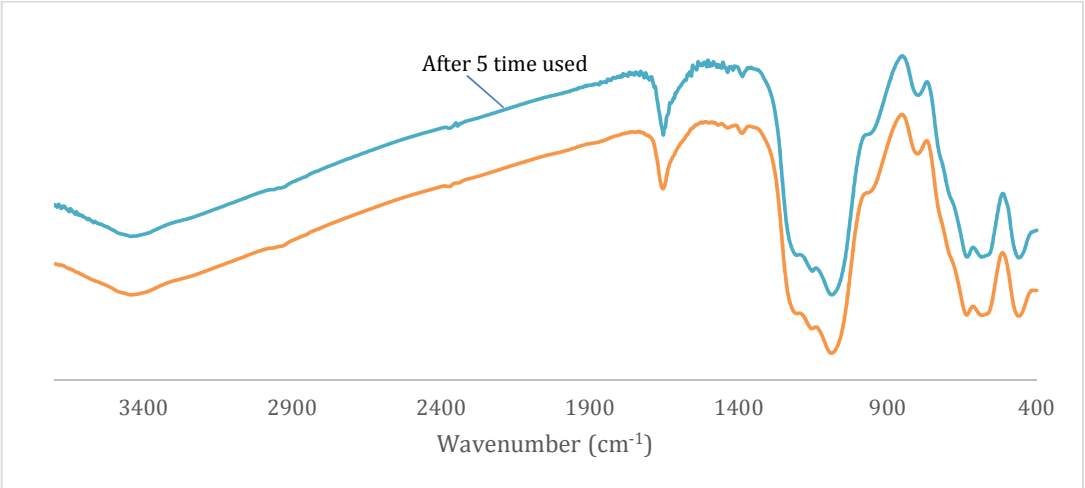

Figure 9. FTIR spectra of fresh and reused catalyst.

Proposed mechanism

The proposed mechanism for the synthesis of 3-aryl-imidazo[1,2-*a*]pyridines from the reaction between phenacyl bromides and 2-aminopyridine in the presence of catalytic amounts of FLU-functionalized magnetic heterogeneous nanocatalyst (0.03 g) is summarized in Scheme 4. The nucleophilic and basic natures of the triazole[22,23] corresponded with reactivity of the catalyst in nucleophilic substitution of bromide in phenacyl bromide and hydrogen abstraction of the intermediate compounds to afford an imidazole ring via a ring closure process.

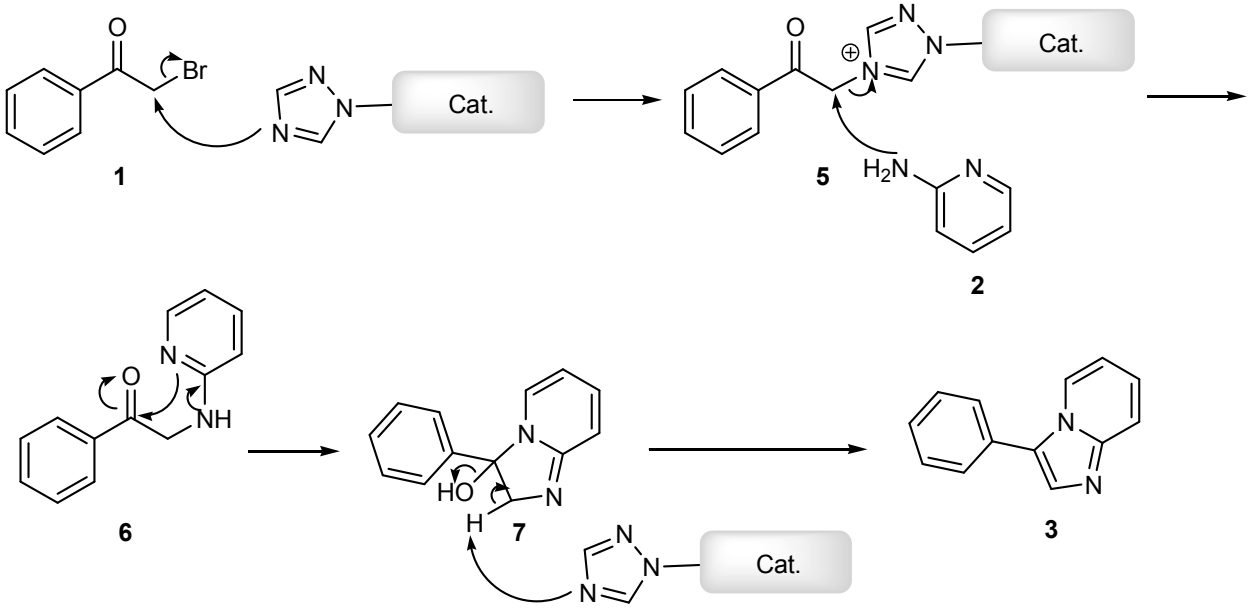

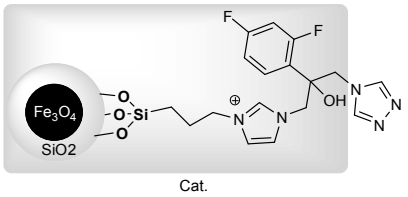

Cat.

Scheme 4. Possible mechanism of the synthesis of 3-aryl-imidazo[1,2-*a*]pyridines in the presence of Fe_3O_4@SiO_2~FLU.

4. Conclusion

This work reported on the preparation of Fe_3O_4@SiO_2~FLU via functionalization of silica-coated magnetic nanoparticles with chloropropyltriethoxysilane (CPTES) as a linker for the immobilization of fluconazole. A Supported Ionic Liquid Phase (SILP) catalyst was also formed upon FLU immobilization. The core-shell nanoparticles were stable and reusable, and the non-toxic and inexpensive heterogeneous nanocatalyst prepared has great potential for applications in organic syntheses. The Fe_3O_4@SiO_2~FLU nanoparticles were developed as a basic/nucleophilic catalyst for the synthesis of different 3-aryl-imidazo[1,2-*a*]pyridines with phenacyl bromides and 2-aminopyridines in water as a solvent. In addition, the catalytic system was applied in a one-pot, three-component coupling reaction of aromatic aldehyde, 2-aminopyridine, and isocyanide in a solvent-free condition to afford substituted 3-amino-imidazo[1,2-*a*]pyridines with excellent yields. The existence of ionic liquid as a medium on the surface (in the absence of a common solvent) may accelerate the accessibility of reactants to catalytic sites (particularly in one-pot/three-component reactions), leading to excellent yields (90-99%). The major advantage of this catalyst was its ease of the recovery, allowing it to be reused without significant change in its catalytic activity.

Acknowledgements

The authors gratefully acknowledge the financial support and technical support from Razi University, University Sains Malaysia (through the USM Short Term Grant no 304/PKIMIA/6312088) and Universiti Malaysia Sabah.

References

1. (a) R. K. Iller, *The Chemistry of Silica*, John Wiley & Sons: New York, 1979; (b) K. D. Kim, S. S. Kim, Y.-H. Choa, H. T. Kim, *J. Ind. Eng. Chem.* **2007,** *13*, 1137-1141; (c) M. Jafarzadeh, R. Adnan, M. K. N. Mazlan, *J. Non-Cryt. Solid* **2012,** *385*, 2981-2987.

2. (a) J. Wang, B. Xu, H. Sun, G. Song, *Tetrahedron Lett.* **2013,** *54*, 238-241; (b) B. Li, L. Gao, F. Bian, W. Yu, *Tetrahedron Lett.* **2013,** *54*, 1063-1066; (c) A. Maleki, *Tetrahedron Lett.* **2013,** *54*, 2055-2059; (d) J. Lee, Y. Lee, J. K. Youn, *Biocomp. Mater.* **2008,** *4*, 143-152; (e) E. Kim, J. Jang, J. S. Chung, *Macromol. Res.* **2014,** *22*, 864-869; (f) S.-D. Pan, H.-Y. Shen, L.-X. Zhou, X.-H. Chen, Y.-G. Zhao, M.-Q.

Cai, M.-C. Jin, *J. Mater. Chem. A* **2014,** *2*, 15345-15356; (g) B. Guoyi, L. Xingwang, L. Xiaofang, *Green Chem.* **2014,** *16*, 3160; (h) A. Palani, J. S. Lee, *J. Proteome Res.* **2008,** *7*, 3591-3596.

3. (a) I. A. Rahman, M. Jafarzadeh, C. S. Sipaut, *J. Sol-Gel Sci. Technol.* **2011,** *59*, 63-72; (b) C. Hui, C. Shen, J. Tian, L. Bao, H. Ding, C. Li, Y. Tian, X. Shi, H.-J. Gao, *Nanoscale* **2011,** *3*, 701-705.

4. (a) J. Q. Wang, L. Huang, *J. Phys. Chem. C* **2008,** *112*, 5014-5022; (b) A. Farook, M. H. Kasim, O. Hasnah, *Appl. Catal. A* **2009,** *365*, 165-172.

5. M. R. Caira, K. A. Alkhamis, R. M. Obaidat, *J. Pharm. Sci.* **2004,** *93*, 601-611.

6. (a) A. B. Ramesha, G. M. Raghavendra, *Tetrahedron Lett.* **2013,** *54*, 95-100; (b) V. M. Bangade, B. C. Reddy, *Tetrahedron Lett.* **2013,** *54*, 4767-4771; (c) A. Shaabani, E. Soleimani, A. Maleki, *Tetrahedron Lett.* **2006,** *47*, 3031-3034; (d) O. P. Pereshivko, V. A. Peshkov, *Synlett* **2013,** 351; (e) A. Shaabani, E. Soleimani, A. Maleki, J. Moghimi-Rad, *Synth. Commun.* **2008,** *38*, 1090-1095; (f) H. Daemi, R. R. Rad, M. Barikani, M. Adib, *Appl. Catal. A* **2013,** *468*, 10-17.

7. L. Chen, Z. Xu, H. Dai, S. Zhang, *J. Alloys Compd.* **2010,** *497*, 221-227.

8. W. Stöber, A. Fink, E. Bohm, *J. Colloid Interface Sci.* **1968**, *26*, 62-69.

9. F. Adam, H. Osman, K. M. Hello, *J. Colloid Interface Sci.* **2009**, *331*, 143–147.

10. A. Riisager, B. Jørgensen, P. Wasserscheid, R. Fehrmann, *Chem. Commun.* **2006,** 994-996.

11. A. Riisager, R. Fehrmann, M. Haumann, P. Wasserscheid, *Eur. J. Inorg. Chem.* **2006,** 695-706.

12. S. Chandrasekhar, B. Tiwari, B. B. Parida, Ch. R. Reddy, *Tetrahedron: Asym.* **2008,** *19*, 495-499.

13. S. Chandrasekhar, T. P. Kumar, K. Haribabu, Ch. R. Reddy, *Tetrahedron: Asym.* **2010**, *21*, 2372-2375.

14. H. Chao, S. Chengmin, T. Jifa, *Nanoscale* **2011,** *3*, 701-705.

15. P. Scherrer, *Göttinger Nachrichten Gesel* **1918,** *2*, 98.

16. V. Balakrishnan, H. A. A. Wab, K. A. Razak, S. Shamsuddin, *J. Nanomater.* **2013**, 729306.

17. Y. Ahn, E. J. Choi, E. H. Kim, *Rev. Adv. Mater. Sci.* **2003,** *5*, 477-480.

18. S. Ahmad, U. Riaz, A. Kaushik, J. Alam, *J. Inorg. Organomet. Polym.* **2009,** *19*, 355-360.

19. M. Yamaura, R. L. Camilo, L. C. Sampaio, M. A. Macêdo, M. Nakamura, H. E. Toma, *J. Magn. Magn. Mater.* **2004,** *279*, 210–217.

20. R.-Y. Hong, J.-H. Li, S.-Z. Zhang, *Appl. Surf. Sci.* **2009,** *255*, 3485-3492.

21. R. J. Hunter, *Zeta Potential in Colloids Science*, Academic Press: 1981.

22. Y.-W. Zhu, W.-B. Yi, C. Cai, *J. Fluorine Chem.* **2011,** *132*, 71-74.

23. C. Tirler, L. Ackermann, *Tetrahedron* doi:10.1016/j.tet.2015.02.033